한국해양환경 · 에너지학회지
J. Korean Soc. Mar. Environ. Energy
Vol. 27, No. 2, 101-110, May 2024

https://doi.org/10.7846/JKOSMEE.2024.27.2.101
ISSN 2288-0089(Print) / ISSN 2288-081X(Online)

Original Article

광양만 개발로 인한 조석 및 조류 변화 특성

김차겸[1,†] · 윤은찬[2]
[1]경남도립남해대학교 산업안전관리과 교수
[2]한국해양수산연구원 책임연구원

The Change of Tide and Tidal Current Due to the Development of the Kwangyang Bay, Korea

Cha-Kyum Kim[1,†] and Eun Chan Yoon[2]
[1]*Professor, Department of Industrial Safety Engineering, University of Gyeongnam Namhae, Namhae 52422, Korea*
[2]*Senior Research Scientist, Korea Ocean and Fisheries Institute, Busan 48280, Korea*

요 약

한국의 남해안에 위치한 광양만은 1982년에 시작된 광양항의 건설로 인해 심각한 환경변화를 겪고 있다. 광양만의 개발로 인한 물리적 영향을 평가하기 위해 김 등(1999)에 의해 개발된 3차원 layer-level 혼성 해수유동 모델을 광양만에 적용하여 광양만 개발 전.후의 조위, 조류 및 조석잔차류의 변화특성을 시뮬레이션하였다. 또한, 1995년 12월부터 2008년 3월까지 주변해역에서 광범위한 해수유동이 조사되었다. 광양만 개발 후 광양만의 입구인 여수수로에서 조류는 광양만 개발 전에 비해 감소하였으나, 광양만의 북측인 섬진강으로 향하는 흐름과 동측인 노량수로로 향하는 흐름은 개발 전에 비해 증가되었다. 조위는 모든 비교 정점에서 개발 후가 개발 전에 비해 증가되었다.

Abstract – The Kwangyang Bay (KB), located in the south sea of Korea, has been undergoing severe environmental changes due to the construction of Kwangyang Harbor started in 1982. A three-dimensional layer-level hybrid model developed by Kim *et al*. (1999) was applied to the KB to estimate the impact of the development of the bay. The simulations were performed to quantify the changes of tidal elevation, tidal current and tidal residual current before and after the development of the KB. In addition, extensive and intensive field measurements on the hydrodynamic conditions have been carried out around the KB from December 1995 to March 2008. Tidal currents at the bay entrance (Yeosu Channel) after the development of the KB decreased whereas the currents at the northern (Sumjin River estuary) and the eastern (Noryang Channel) parts of the bay showed increase compared to the condition before the development. The tidal elevations after the development at all comparison Stations increased as compared with those before the development.

Keywords: Kwangyang Bay(광양만), tide(조석), tidal current(조류), numerical model(수치모델)

1. Introduction

Kwangyang Bay (hereafter, KB) is located in the central south sea of Korea, and the water exchange of the bay with the ocean occurs through Yeosu Channel (hereafter, YC) and Noryang Channel (hereafter, NC) (see Fig. 1). The geometry is complex and the depth is less than 35 m in general. The width at the narrowest site of the NC is about 500 m, and the narrowest width of the YC is about 3 km. The bay is connected to the Sumjin (Seomjin) River toward the north. The averaged annual discharge of the Sumjin River is about 120 m^3/sec, and the design flood discharge of 100 years occurrence frequency is 12,000 m^3/sec. The KB has been undergoing severe topographic and geographic changes due to the construction of Kwangyang Harbor started in 1982. The expansion projects of the Kwangyang Harbor for the container and dumping sites are in progress. The intertidal flat in Sumjin River estuary has been destroyed due to sand mining and dredging. The depth

†Corresponding author: kick@namhae.ac.kr

(Fig. 1) after the development of the KB is deeper than that (Fig. 2) before the development. The water depth before the development in Sumjin River estuary is less than 1 m, and suitable for navigation of small ships only, whereas the depth after the development is more than 3 m due to the dredging for the construction of the Kwangyang Harbor. Compared with the condition before the development of the KB, the salt intrusion has strongly developed to the upstream part of the Sumjin River, and therefore groundwater is suffering the salt pollution from sea water(Lee *et al.*[2008]; Na and Son[2005]; Noh *et al.*[2011]; Lee *et al.*[2022]). This study is focused to understand the changing conditions of tide, tidal current and tidal residual current due to the development of the KB using a three-dimensional numerical model(Kim *et al.*[1999]). Kim[2003, 2005] investigated the hydrodynamic, water quality and sediment transport in the KB using the 3-D layer-level hybrid model developed by Kim *et al.*[1999]. Kim *et al.*[2010] analyzed the water circulation structure in the Chinju (Jinju) Bay, and Kim[2013] carried out the 3-D numerical simulations of the hydrodynamic circulation and the impact of the freshwater runoff in the Chinju Bay. Kim *et al.*[2002] used 3-D model to investigate tidal current change and effluent pattern from Sumjin River due to the development of the KB. Ro[2007] analyzed the characteristics of tidal and sub-tidal currents in the Kangjin Bay, and Ro *et al.*[2010] carried out numerical modeling experiments to study the impact of the dam water discharge on the circulation system in the Kangjin Bay. Kim *et al.*[2008] studied three-dimensional mixing characteristics in Seomjin (Sumjin) River estuary using the EFDC model and seasonal field data during spring

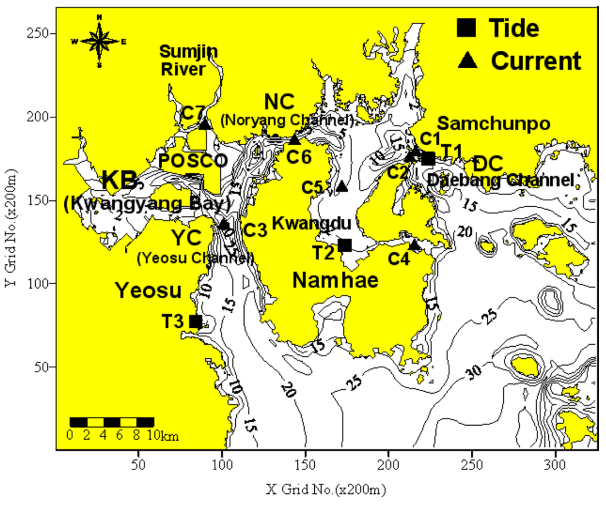

Fig. 1. Model domain and data sites after the development of Kwangyang Bay.

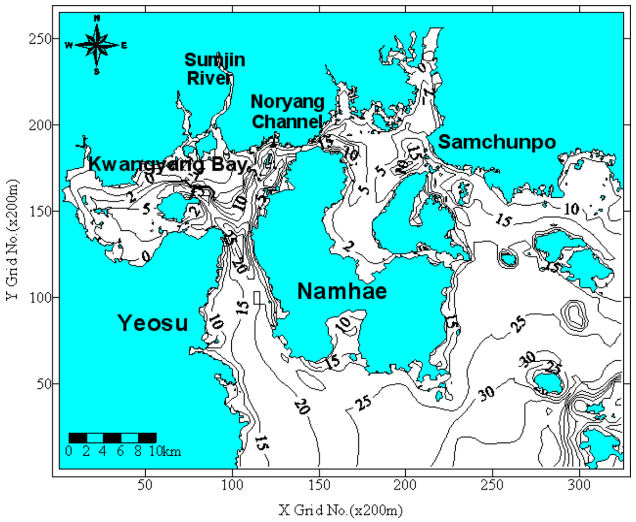

Fig. 2. Model domain before the development of Kwangyang Bay.

tide. Kang *et al.*[2011] simulated three-dimensional ocean circulation patterns using the EFDC model in the KB and Jinju (Chinju) Bay. Kim *et al.*[2014] used ECOM-3D to investigate the circulation characteristics in Kwangyang Estuarine system. The main purpose of the present study is to simulate the tidal elevation, tidal current and tidal residual current before (Fig. 2) and after (Fig. 1) the development of the KB using 3-D hybrid model (Kim *et al.*[1999]), and to estimate the impact of the development of the KB.

2. Field Measurements

Tidal elevations at Sts. T1 and T3 (Fig. 1) were observed at a time interval of 10 minutes with SBE 26 tide gauge (made in USA). The measurements at Sts. T1 and T3 were carried out in period of December 2, 1995 ~ January 11, 1996, and the data at St. T2 (Fig. 1) are those obtained from KHOA (Korea Hydrographic and Oceanographic Agency) during the same period (Kim *et al.*[2002]).

Flow velocity was measured at a time interval of 10 minutes with ADCP and RCM-9 current meters. The measurements of the flow velocity at St. C3 (Fig. 1) were carried out in the period of December 2, 1995 ~ January 11, 1996, and the measurements at St. C6 (Fig. 1) were carried out on November 22 ~ December 13, 1998, May 7 ~ May 26, 2005 and January 29 ~ March 1, 2008. More detailed informations on the field work and the data are given in Kim *et al.*[2002] and Kim *et al.*[2010].

3. Numerical Model

3.1 Governing equations

Assuming the hydrostatic pressure distribution and the Boussinesq approximation, the governing equations in a three-dimensional (x, y, z) coordinate system with z-axis vertically upwards are:

$$\frac{\partial u}{\partial x}+\frac{\partial v}{\partial y}+\frac{\partial w}{\partial z}=0 \tag{1}$$

$$\frac{\partial u}{\partial t}+u\frac{\partial u}{\partial x}+v\frac{\partial u}{\partial y}+w\frac{\partial u}{\partial z}=fv-\frac{1}{\rho_o}\frac{\partial p}{\partial x}\frac{\partial}{\partial x}(\epsilon_x\frac{\partial u}{\partial x})+\frac{\partial}{\partial y}(\epsilon_y\frac{\partial u}{\partial y})+\frac{\partial}{\partial z}(\epsilon_z\frac{\partial u}{\partial z}) \tag{2}$$

$$\frac{\partial v}{\partial t}+u\frac{\partial v}{\partial x}+v\frac{\partial v}{\partial y}+w\frac{\partial v}{\partial z}=-fu-\frac{1}{\rho_o}\frac{\partial p}{\partial y}+\frac{\partial}{\partial x}(\epsilon_x\frac{\partial v}{\partial x})+\frac{\partial}{\partial y}(\epsilon_y\frac{\partial v}{\partial y})+\frac{\partial}{\partial z}(\epsilon_z\frac{\partial v}{\partial z}) \tag{3}$$

$$\frac{\partial p}{\partial z}=-\rho g \tag{4}$$

where u, v and w are the velocity components in x, y and z directions respectively; t is the time; p is the pressure; f is Coriolis parameter as $2\Omega\sin\theta$ where θ is the latitude; Ω is the angular speed of earth rotation; g is the gravity; ρ_c is the reference density; ρ is the water density; ε_x, ε_y and ε_z are the turbulent eddy coefficients in x, y and z directions, respectively. After substituting equation (4) into equations (2) and (3), and taking the vertical integration of equations (1) to (3) for the kth layer, and also using a streamline condition at the surface and the bottom, the governing equations become:

$$\frac{\partial \zeta}{\partial t}+\sum_{k=1}^{b}\{\frac{\partial (uh)_k}{\partial x}+\frac{\partial (vh)_k}{\partial y}\}=0, k=1,2,...,b \tag{5}$$

$$\frac{\partial u}{\partial t}+u\frac{\partial u}{\partial x}+v\frac{\partial u}{\partial y}+\frac{w}{h}(u_{k-1/2}-u_{k+1/2})=fv-g\{\frac{\rho_{k-1}}{\rho_k}\frac{\partial \zeta}{\partial x}+\frac{\rho_k-\rho_{k-1}}{\rho_k}\frac{\partial \eta}{\partial x}\}+\frac{\partial}{\partial x}(\epsilon_x\frac{\partial u}{\partial x})+\frac{\partial}{\partial y}(\epsilon_y\frac{\partial u}{\partial y})+\frac{1}{h}\{(\epsilon_z\frac{\partial u}{\partial z})_{k-1/2}-(\epsilon_z\frac{\partial u}{\partial z})_{k+1/2}\} \tag{6}$$

$$\frac{\partial v}{\partial t}+u\frac{\partial v}{\partial x}+v\frac{\partial v}{\partial y}+\frac{w}{h}(v_{k-1/2}-v_{k+1/2})=-fu-g\{\frac{\rho_{k-1}}{\rho_k}\frac{\partial \zeta}{\partial y}+\frac{\rho_k-\rho_{k-1}}{\rho_k}\frac{\partial \eta}{\partial y}\}+\frac{\partial}{\partial x}(\epsilon_x\frac{\partial v}{\partial x})+\frac{\partial}{\partial y}(\epsilon_y\frac{\partial v}{\partial y})+\frac{1}{h}\{(\epsilon_z\frac{\partial v}{\partial z})_{k-1/2}-(\epsilon_z\frac{\partial v}{\partial z})_{k+1/2}\} \tag{7}$$

where ζ is the displacement of the free surface; h is the layer thickness; η is the elevation of internal wave; and b represents the bottom layer. The integrated mass conservation equation of salinity transport for the k-th layer is

$$\frac{\partial (hS)}{\partial t}+\frac{\partial (huS)}{\partial x}+\frac{\partial (hvS)}{\partial y}+(wS)_{k-1/2}-(wS)_{k+1/2}=\frac{\partial}{\partial x}(D_x h\frac{\partial S}{\partial x})+\frac{\partial}{\partial y}(D_y h\frac{\partial S}{\partial y})+(D_z\frac{\partial S}{\partial z})_{k-1/2}-(D_z\frac{\partial S}{\partial z})_{k+1/2} \tag{8}$$

where S is the salinity; D_x and D_y are horizontal eddy diffusivity; D_z is the vertical eddy diffusivity.

The continuity equation for the computation of internal elevation is

$$\frac{\partial \eta_k}{\partial t}+\frac{\partial (uh)_k}{\partial x}+\frac{\partial (vh)_k}{\partial y}+Q=0, k=1,2,...,b \tag{9}$$

where Q is the transport flux of water mass from lower layer to upper layer, and Q can be written as

$$Q=E\{\sqrt{u_k^2+v_k^2}-\sqrt{u_{k+1}^2+v_{k+1}^2}\}$$

$$E=\frac{4.34\times 10^{-3}}{0.0578+Ri^{3/2}}$$

$$Ri=\frac{g(\rho_{k+1}-\rho_k)h}{\rho(u_k^2+v_k^2)}$$

The vertical velocity can be computed as

$$w_{k+1/2}=\sum_{l=k}^{b}\{\frac{\partial (uh)_l}{\partial x}+\frac{\partial (vh)_l}{\partial y}\}=0 \tag{10}$$

3.2 Numerical solution

The KB was simulated with a three-dimensional numerical model (Kim *et al.*[1999]; Kim *et al.*[2002]; Kim[2003]; Kim[2005]; Kim[2013]) using an ADI (Alternating Direction Implicit) finite difference scheme. The time step is 20 sec (based on the CFL condition), the horizontal grid size is 200 m, and the area is discretized by 260 × 325 points in the horizontal and 4 layers over the depth, the vertical grid size varies from 2 to 10 m. The land boundaries are assumed impermeable where the normal component of velocity is set to zero. On river boundaries, the flow rate is given as 120 m^3/sec. At closed boundaries the transport of substance is zero. At an open boundary the concentration must be specified during inflow. On outflow the substance is advected out of the model domain. In order to drive the hydrodynamic model, water elevation data were used at seaward boundary. The open boundaries for each grid are forced by linear interpolation with M_2, S_2, K_1 and O_1 tidal constituents.

4. Results and Discussions

4.1 Measured tidal height

Tides in the KB are predominantly semi-diurnal. The results of harmonic analyses of tides at Sts. T1, T2 and T3 are compared in Table 1 (Kim *et al.*[2002]). Only 4 constituents (M_2, S_2, K_1 and O_2) are presented. Amplitudes of M_2-tide are everywhere predominant, and S_2 components are approximately one-half of the M_2 components. The amplitudes of two diurnal components, O_1 and K_1, are very small. Tides at Yeosu Harbor

Table 1. Comparisons of tides at Sts. T1~T3 (Kim *et al.*[2002])

Tide	Period (hr)	St. T1 (Samchunpo)		St. T2 (Kwangdu)		St. T3 (Yeosu)	
		Amp. (cm)	G. Phase (°)	Amp. (cm)	G. Phase (°)	Amp. (cm)	G. Phase (°)
M_2	12.42	92.0	341.1	105.2	7.9	99.7	359.6
s_2	12.00	44.3	5.6	51.2	36.5	45.3	24.9
K_1	23.93	15.6	42.1	20.6	51.4	18.4	49.7
O_1	25.82	12.4	22.6	12.0	25.7	12.7	29.9

Table 2. Harmonic constants of the east-west component of tidal current at St. C6 during August 31~October 2, 2007 (Kim *et al.*[2010])

Position	Constituents	Amp. (cm/sec)	Phase lag (°)
Surface layer (5m from surface)	M_2	73.92	230.80
	S_2	41.48	255.44
	K_1	11.90	158.32
	O_1	8.37	135.40

Table 3. Harmonic constants of the north-south component of tidal current at St. C1 during April 14 ~ May 16, 2005 (Kim *et al.*[2010])

Position	Constituent	Amp. (cm/sec)	Phase lag (°)
Surface layer (5 m from surface)	M_2	90.26	167.97
	S_2	37.54	202.23
	K_1	7.33	75.03
	O_1	5.96	15.50

(St. T3) lag behind those at Samchunpo (Samcheonpo) Harbor (St. T1) by 38.3 minutes for M_2-tide.

4.2 Measured tidal current

Extensive and intensive measurements during long period were carried out at Sts. C1, C2, C3 and C6 (Kim *et al.*[2002]; Kim *et al.*[2010]. Table 2 is the result of harmonic analysis for tidal current at the 5 m depth of St. C6. M_2 and S_2 amplitudes are 73.92 and 41.48 cm/sec, respectively. M_2 and S_2 amplitudes at St. C1 (Table 3) are 90.26 and 37.54 cm/sec, respectively. Tidal form factors at Sts. C6 and C1 are 0.13~0.18 and 0.10~0.11, respectively (Kim *et al.*[2010]). The semi-diurnal tidal currents are dominated, and the S_2 components are approximately one-half of the M_2 components.

4.3 Comparisons of tide and tidal current

The computations were conducted to reproduce the tidal elevation during the period from September 25 to October 26, 2003 at St. T3 (Yeosu Harbor). Fig. 3 shows a comparison of measured and computed tidal profiles at Yeosu Harbor. The computed tidal profile is in good agreement with the measurements. Fig. 4 shows that the computed profiles of tidal currents at St. C6 (NC) are in good agreement with the measurements. The solid line is the computed results and the dotted line is the measurements.

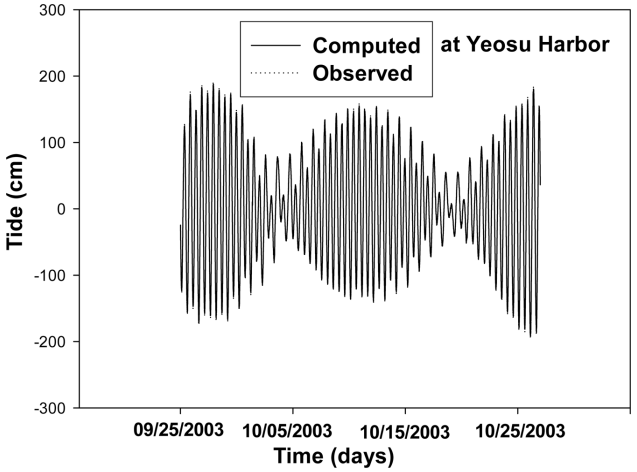

Fig. 3. Comparison of tidal profiles at St. T3 (Yeosu Harbor) from September 25 to October 26, 2003.

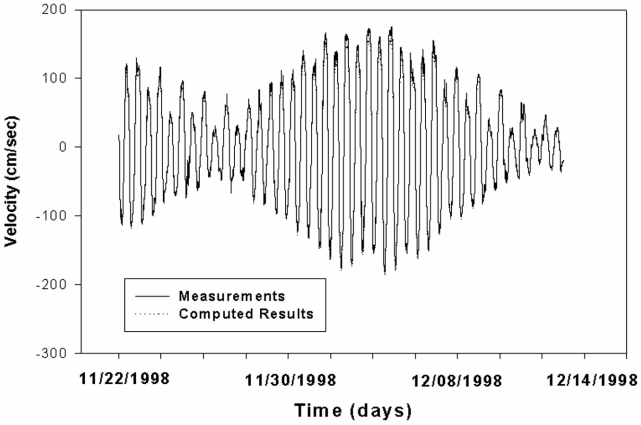

Fig. 4. Comparison of tidal current profiles at St. C6 (NC).

The model was validated using tidal elevation measurements at St. T3 (Yeosu Harbor), and velocity measurements at the NC. The model successfully reproduced the tidal profile at St. T3 and the current profile observed at the NC (St. C6).

4.4 Computed tidal current

A 3-D numerical model was used to estimate the impact of the development of the KB. The water elevations were initially set to mean water level everywhere and the initial velocities were set to zero. The initial salinity level was set at 32 ppt

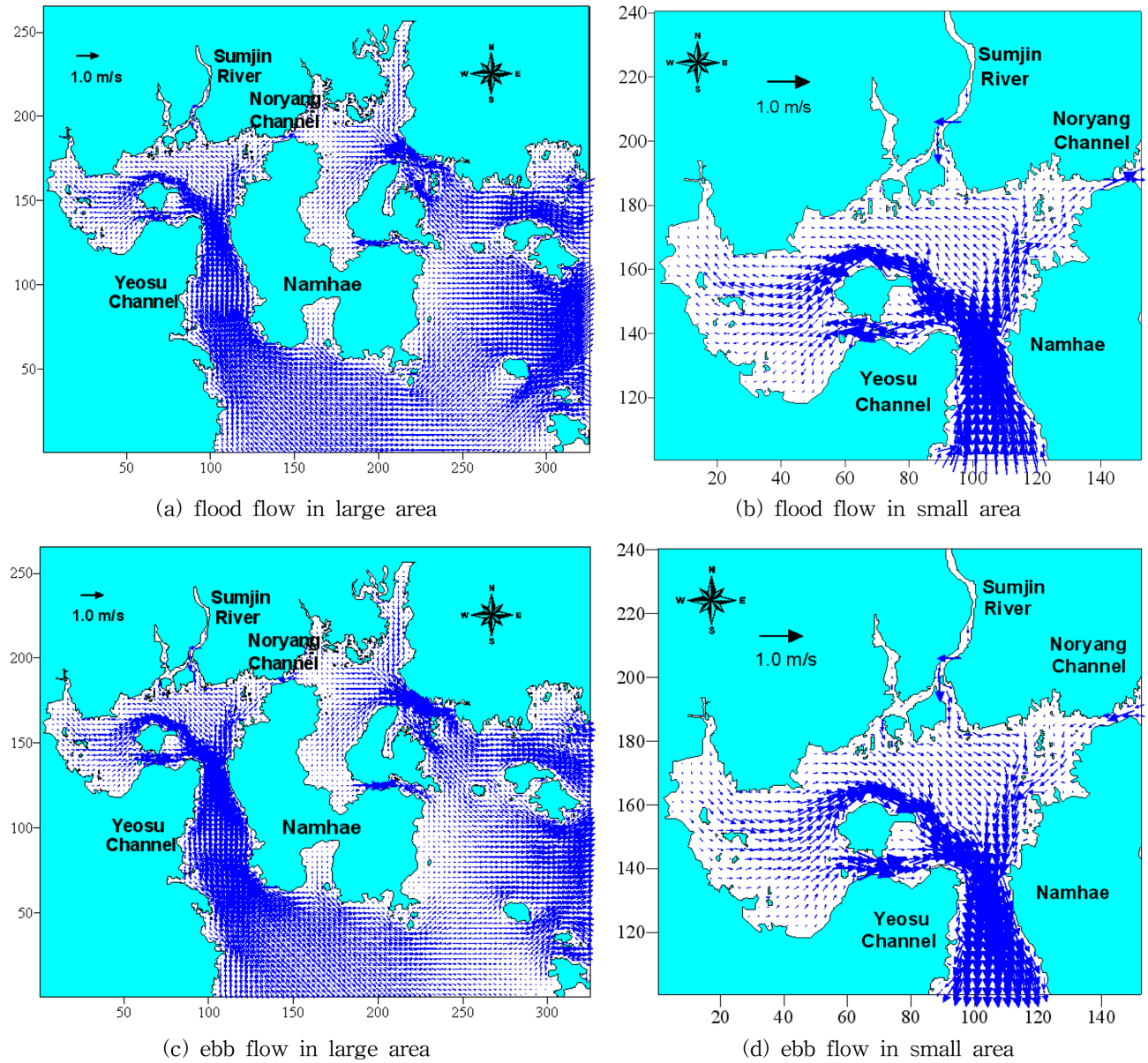

Fig. 5. Computed velocity fields at surface layer during the spring tide in large and small area before the development of the KB.

everywhere. The predicted results were verified with field observations. The model was run with four tidal harmonic constants (M_2, s_2, K_1 and O_1) for 31 days. The system went to equilibrium after about one tidal cycle.

Fig. 5(a, b, c and d) and Fig. 6(a, b, c and d) show the computed current fields at the surface layer during the spring flood tide and the ebb tide in large and small area before and after the development of the KB, respectively. The tidal currents at the YC are predominantly north-south directions, whereas the currents at the NC are east-west directions, and in general, the currents parallel to the coastlines. Upstream of the KB mouth is divided into tri-direction (westward, northward and eastward) during flood tide and this pattern is reversed during ebb tide. The flood flow at YC is northward, whereas the ebb flow is southward. The highest velocity occurs at the NC (St. C6), whereas the velocity at the central part of the KB is much smaller than at the YC and the NC during the flooding and ebbing. The maximum current speed at the YC during flood tide is 86 cm/sec, and the maximum speed during ebb tide reaches up to 96 cm/sec. The observed maximum current speed during the spring tide at the NC is approximately 1.8 m/sec westward, whereas the computed maximum velocity is approximately 1.9 m/sec westward. The ebb velocity is usually larger than the flood velocity, and the tidal flow during wet season is stronger

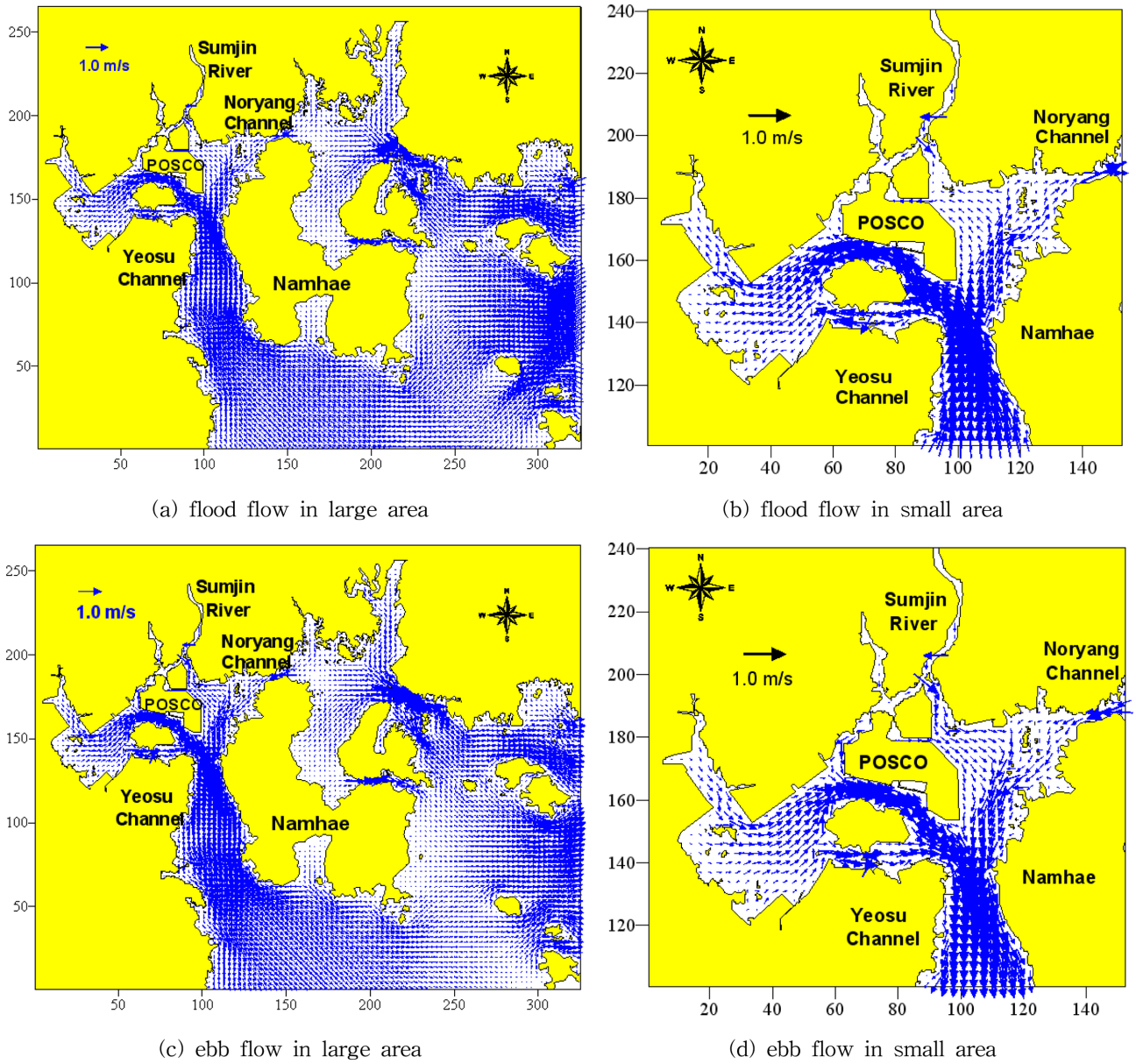

Fig. 6. Computed velocity fields at surface layer during the spring tide in large and small area after the development of the KB.

than during dry season. Due to the influence of the river inflow and the action of the bottom resistance, the tidal wave in Sumjin (Seomjin) River estuary deforms during the upstream propagation, resulting in shorter flood duration and longer ebb duration.

4.5 Comparisons of hydrodynamic change before and after the development

Fig. 7(a, b and c) show the computed velocity profiles before and after the development of the KB at the surface layer of Sts. C3 (YC), C6 (NC) and C7 (Sumjin River estuary), respectively. As the major component of the flow at the Sts. C3 (YC) and C7 (Sumjin River estuary) is a north-south velocity, the comparisons of the north-south component of the velocity are presented. Also, as the flow at St. C6 (NC) is predominant eastward during flood tide and westward during ebb tide, the comparisons of the east-west velocity are presented. The current speed after the development at St. C3 (YC) decreased as compared with those before the development due to the reduction of tidal volume at the bay entrance. The flow velocity after the development at St. C6 (NC) showed increase compared with those before the development. This phenomenon is attributed to the decreased tidal volume of the western KB due to the development. When the tidal current go to the KB, the

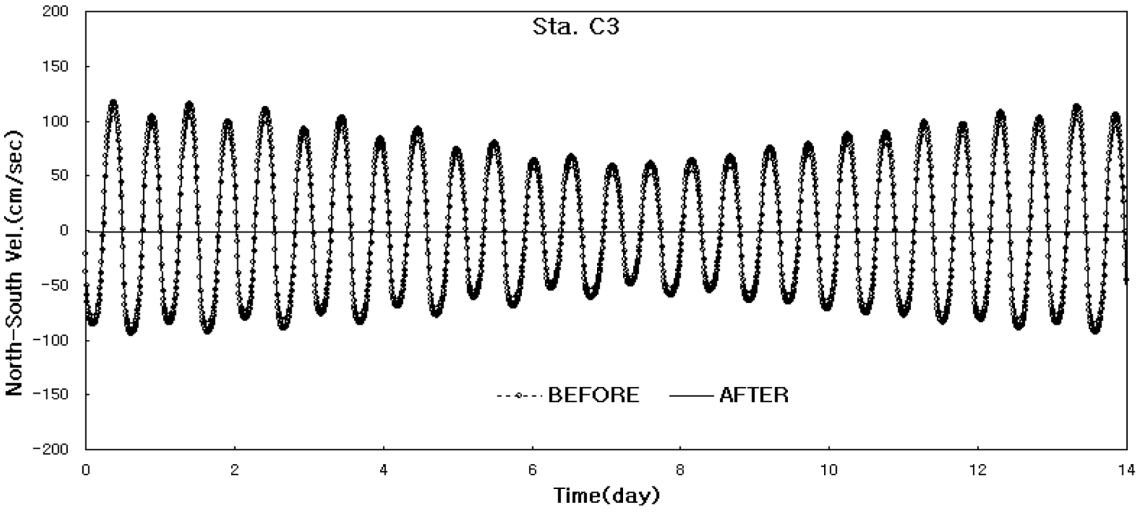

(a) the amplitude of north-south velocity at St. C3 (YC)

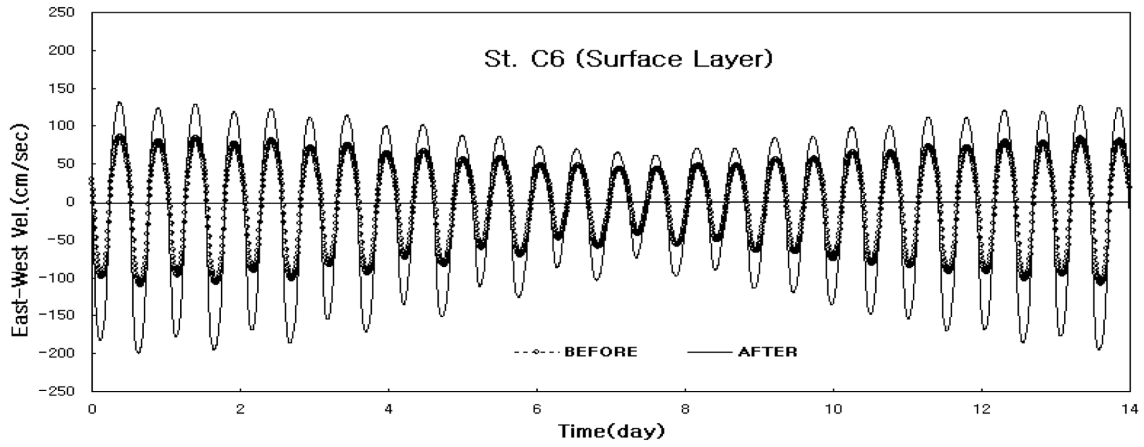

(b) the amplitude of east-west velocity at St. C6 (NC)

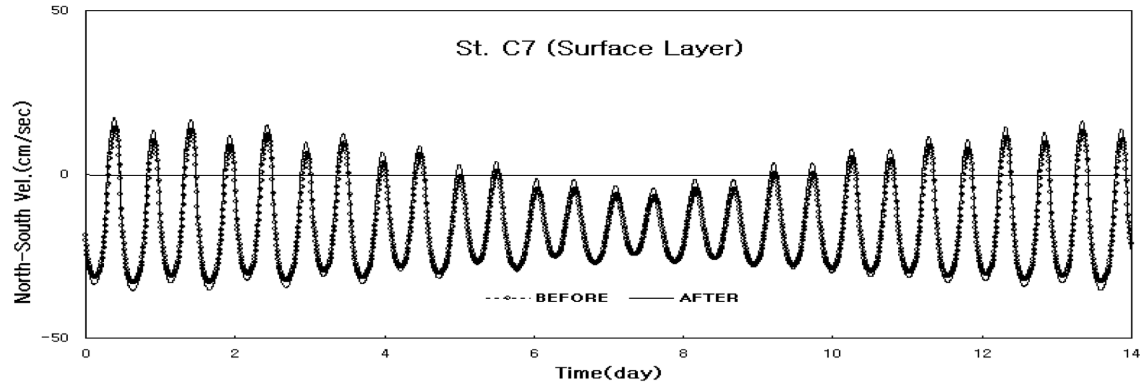

(c) the amplitude of north-south velocity at St. C7 (Sumjin River estuary)

Fig. 7. Comparisons of the current speed at Sts. C3 (YC), C6 (NC) and C7 (Sumjin River estuary) before and after the development of the KB.

current are divided into the tri-direction (northward, westward and eastward). After the development westward tidal volume decreased due to the reduced water area. Therefore, the tidal current go predominantly northward (St. C7) and the NC (St. C6). The flow after the development at St. C6 (NC) and C7 (Sumjin River estuary) is much stronger than before the development due to the increased tidal volume. Tidal volume after the development at Sts. C6 (NC) and C7 (Sumjin River

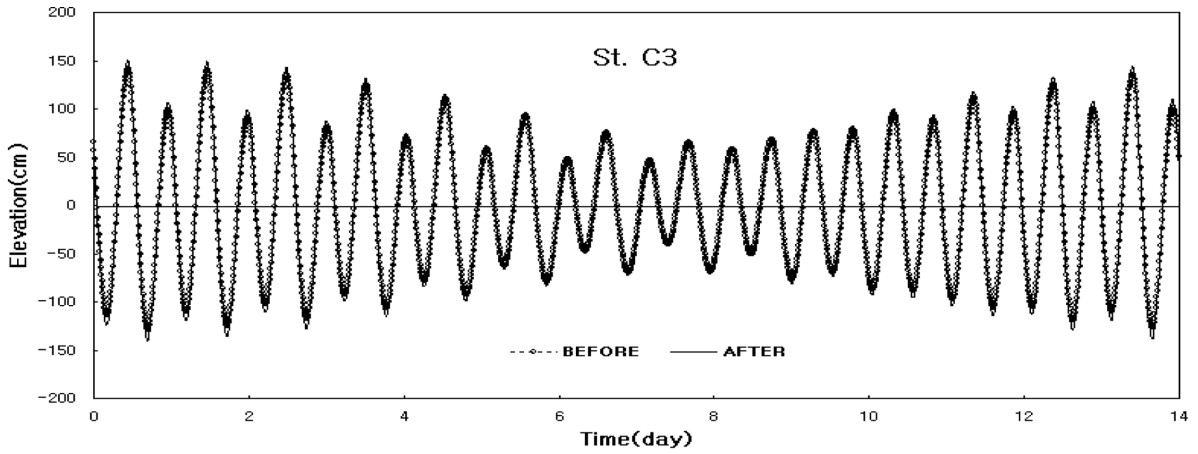

(a) the tidal amplitudes at St. C3 (YC)

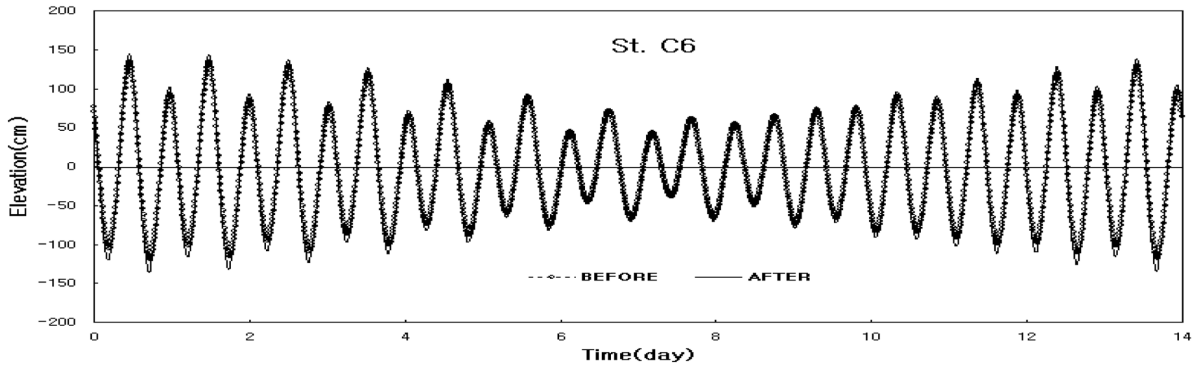

(b) the tidal amplitudes at St. C6 (NC)

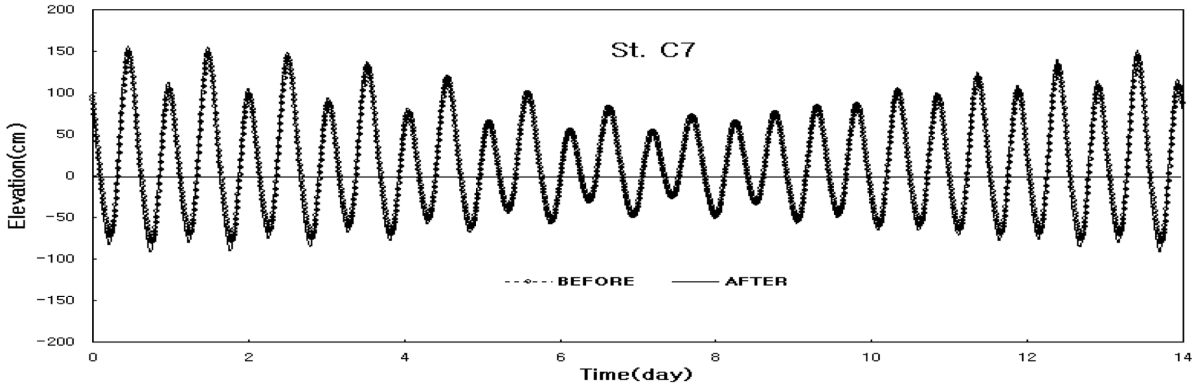

(c) the tidal amplitudes at St. C7 (Sumjin River estuary)

Fig. 8. Comparisons of the tidal amplitudes at Sts. C3 (YC), C6 (NC) and C7 (Sumjin River estuary) before and after the development of the KB.

estuary) increased whereas the volume at St. C3 (YC) decreased as compared with the volume before the development.

Fig. 8(a, b and c) show the comparisons of tidal amplitudes at Sts. C3 (YC), C6 (NC) and C7 (Sumjin River estuary) before and after the development of the KB. The tidal elevations after the development at all Stations increased as compared with those before the development due to the decreased water area in the KB.

4.6 Computed tidal residual current

Fig. 9(a and b) show the computed tidal residual currents at surface layer before and after the development. The residual flow is strongest on the Sumjin (Seomjin) River estuary and is progressively weaker toward the south. The residual currents in Sumjin River estuary flow southward due to the discharge of the freshwater from the Sumjin River. The small scale eddy occurs at the west of the NC, and the residual currents at the

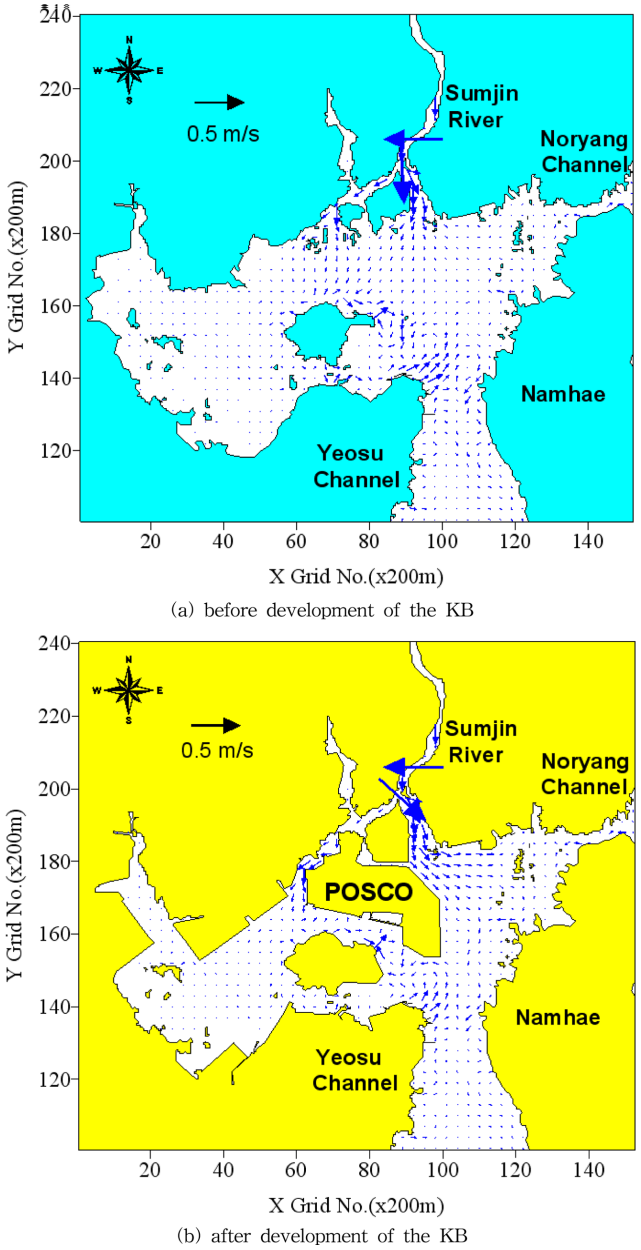

Fig. 9. Computed tidal residual currents at surface layer before and after the development of the KB.

northwestern part of the YC rotate counterclockwise throughout 30 days cycle. The residual currents at east side of the POSCO after the development are much stronger than before the development, and the increased currents can cause sediments to erode. The residual currents in the model domain vary greatly depending on the coastal structure after the development, the location and the bottom topography. Furthermore, the residual currents in Sumjin River estuary after the development were strengthened as compared with the residual currents before the development. Due to the influence of the river inflow, the ebb flow in Sumjin River estuary has been enhanced causing seasonal residual sediment transport(Kim[2005]). According to Choo[2002], the changes of kinematic energy including tidal residual currents, density currents and wind driven currents due to the coastal development of the KB were reduced by 10% compared with before the coastal development.

5. Conclusions

A three-dimensional layer-level hybrid model was applied to the KB located in the south sea of Korea to estimate the impact of the development of the bay. The simulations were performed to quantify the changes of tidal elevation, tidal current and tidal residual current before and after the development the KB. Tidal currents at the bay entrance (YC) after the development of the KB decreased whereas the currents at the northern (Sumjin River estuary) and the eastern part (NC) of the bay showed increase compared to the conditions before the development. The tidal elevations after the development at all comparison Stations (YC, NC and Sumjin River estuary) increased as compared with those before the development. This model can be used as an important tool to study the impact over hydrodynamic and ecological system which require further detailed investigation.

References

[1] Choo, H.S., 2002, Numerical experiment for the changes of currents by reclamation of land in Kwangyang Bay, J. Environmental Sciences, 11(7), 637-650.

[2] Kang, Y.S., Chae, Y. and Lee, H.R., 2011, Variation of density stratification due to fresh water discharge in the Kwangyang Bay and Jinju Bay, J. Korean Society of Coastal and Ocean Engineers, 23(1), 126-137.

[3] Kim, B.K., Ro, Y.J., Jung, K.Y. and Park, K.S., 2014, Numerical modeling of circulation characteristics in the Kwangyang Estuarine system, J. Korean Society of Coastal and Ocean Engineers, 26(4), 253-266.

[4] Kim, C.K., 2003, Three-dimensional hydrodynamic and sediment transport modeling of Kwangyang Bay, South Coast of Korea, in proc. of ECM8, 27.

[5] Kim, C.K., 2005, Sediment transport and river plume modeling in the South Coast of Korea, ISOPE, I, 645-649.

[6] Kim, C.K., 2013, Modeling hydrodynamic circulation and the impact of the freshwater runoff in the Chinju Bay, Korea, in proc. of ECM13, 1.

[7] Kim, C.K., Lee, J.C. and Ro, Y.J., 2002, Tidal current change and effluent pattern from Sumjin River due to the development of Kwangyang Bay, Symposium on Ocean Space Development

and Environmental Preservation Countermeasure in the Southern Coastal Waters of Korea, University of Gyeongnam Namhae, 185-223.

[8] Kim, C.K., Lee, J.T. and Jang, H.S., 2010, Water circulation structure in the Chinju Bay of Korea, J. Korean Society of Coastal and Ocean Engineers, 22(4), 215-223.

[9] Kim, C.K., Yang, H.S. and Kim, K.C., 1999, Development of three-dimensional combined layer and level hydrodynamic model, J. the Korean Society of Civil Engineers, 19(II-5), 603-614.

[10] Kim, J.K., Kwak, G.I. and Jeong, J.H., 2008, Three-dimensional mixing characteristics in Seomjin River Estuary, J. the Korean Society for Marine Environmental Engineering, 11(3), 164-174.

[11] Lee, G.Y., Park, S.C., Park, S.H., Kim, E.S. and Lee, W., 2022, Evaluation of saltwater intrusion at the Sumjin River estuary by numerical model, Korean Society of Water Science & Technology, 30(6), 107-117.

[12] Lee, S.B., Hong, C.O., Oh, J.H., Gutierrez, J. and Kim, P.J., 2008, Effect of irrigation water salinization on salt accumulation of plastic film house soil around Sumjin River estuary, Korean Journal of Environmental Agriculture, 27(4), 349-355.

[13] Na, C.K. and Son, C., 2005, Groundwater quality and pollution characteristics at Seomjin River basin: pollution source and risk assesment, The Korean Society of Economic and Environmental Geology, 38(3), 261-272.

[14] Noh, J., Lee, J.Y. and Shin, J.K., 2011, Analysis of saltwater intrusion by flushing discharge in the Seomjin River estuary, J. Environmental Impact Assessment, 20(3), 325-335.

[15] Ro, Y.J., 2007, Tidal and sub-tidal current characteristics in the Kangjin Bay, South Sea, Korea, Ocean Science Journal, 42(1), 19-30.

[16] Ro, Y.J. and Jung, K.Y., 2010, Impact of the dam water discharge on the circulation system in the Kangjin Bay, South Sea, Korea, Ocean Science Journal, 45(1), 7-25.

Received 10 October 2023
1st Revised 13 November 2023, 2nd Revised 7 December 2023
Accepted 18 December 2023